Frontiers in Heat and Mass Transfer

Tech Science Press

DOI: 10.32604/fhmt.2024.056597

ARTICLE

Nanofluid Heat Transfer in Irregular 3D Surfaces under Magnetohydrodynamics and Multi-Slip Effects

Mumtaz Khan[1,*], Muhammad Shoaib Anwar[2], Mudassar Imran[3] and Amer Rasheed[4]

[1]Faculty of Science, Jiangsu University, Zhenjiang, 212013, China

[2]Department of Mathematics, University of Jhang, Jhang, 35200, Pakistan

[3]College of Humanities and Science, Ajman University, Ajman, 346, United Arab Emirates

[4]Department of Mathematics, School of Science and Engineering, Lahore University of Management Sciences, Lahore Cantt, 54792, Pakistan

*Corresponding Author: Mumtaz Khan. Email: mkhan@ujs.edu.cn

Received: 25 July 2024 Accepted: 13 September 2024 Published: 30 October 2024

ABSTRACT

This study employs the Buongiorno model to explore nanoparticle migration in a mixed convection second-grade fluid over a slendering (variable thickness) stretching sheet. The convective boundary conditions are applied to the surface. In addition, the analysis has been carried out in the presence of Joule heating, slips effects, thermal radiation, heat generation and magnetohydrodynamic. This study aimed to understand the complex dynamics of these nanofluids under various external influences. The governing model has been developed using the flow assumptions such as boundary layer approximations in terms of partial differential equations. Governing partial differential equations are first reduced into ordinary differential equations and then numerically solved using the Runge-Kutta-Fehlberg method (RK4) in conjunction with a shooting scheme. Our results indicate significant increases in Nusselt and Sherwood numbers by up to 14.6% and 23.2%, respectively, primarily due to increases in the Brownian motion parameter and thermophoresis parameter. Additionally, increases in the magnetic field parameter led to a decrease in skin friction coefficients by 37.5%. These results provide critical insights into optimizing industrial processes such as chemical production, automotive cooling systems, and energy generation, where efficient heat and mass transfer are crucial. Buongiorno model; velocity-slip effects; Joule heating; convective boundary conditions; Runge-Kutta-Fehlberg method (RK4).

KEYWORDS

Buongiorno model; velocity-slip effects; Joule heating; convective boundary conditions; Runge-Kutta-Fehlberg method (RK4)

Nomenclature

M	Magnetic parameter
n	Velocity power index parameter
β_1	Second-grade fluid parameter
N_{tp}	Thermophoresis parameter

N_{bm}	Brownian motion parameter
τ_1	Velocity slip parameter
γ_1	Thermal Biot number
γ_2	Concentration Biot number
Pr	Prandtl number
Sc	Schmidt number
Π_{rd}	Radiation parameter
I_H	Internal heat generation parameter
Nu	Heat transfer coefficient
Sh	Mass transfer coefficient
C_{Fx}, C_{Fy}	Frictional resistance coefficient
U_0	Reference velocity
σ	Stefan-Boltzmann constant
k_1	Absorption coefficient
Ec	Eckert number
J	Geometric scaling factor
μ_f	Dynamic viscosity of fluid
k_f	Thermal conductivity of fluid
c_{pf}	Specific heat capacity at constant pressure
D_B	Brownian diffusion coefficient
D_T	Thermophoretic diffusion coefficient
ξ_1	Slip coefficients
h_f, h_w	Transport coefficients
T_∞	External temperature
C_∞	External concentration
T_w	Boundary Temperature
C_w	Boundary concentration
Q_0	Heat generation parameter
B_0	Magnetic field strength
$\chi_{cp} = \frac{(\rho c_p)_p}{(\rho c_p)_f}$	Capacity ratio of particle to fluid

1 Introduction

Nanoparticles, such as particles or fibers dispersed in liquids such as water, oil, or ethylene glycol, belong to an advanced group of solid-liquid substances that have brought significant advancements in the field of thermal science. When mixed with nanoparticles that vary in size from 1 to 100 nanometers, these fluids display altered characteristics. These changes affect thickness, mass, heat transfer efficiency, and distribution patterns. As a result, they offer better rates of heat transfer compared to base fluids. This makes them fascinating in engineering disciplines, including biomechanics, the chemical and nuclear industries, and general engineering applications. However, despite the growing interest and range of applications of nanofluids, their dynamics are still poorly understood. This is especially true for the effects of magnetohydrodynamics (MHD) and surface irregularities on nanofluids. The lack of knowledge in this area is particularly critical for applications that require behavioral control. Our study focuses on bridging this gap in understanding by exploring the thermal transfer processes and three-dimensional movement patterns in a nanofluid that consists of a second-grade fluid. A nanofluid is a class of fluid consisting of a base liquid dispersed with nanoparticles

exhibiting significant enhancement in heat transfer properties. Nanofluids were first postulated by Choi et al. [1] as an unprecedented class of fluids. Since then, considerable advances have been made to this basic notion, then in Eastman et al. [2] an exceptionally high effective thermal conductivity for nanofluids containing ethylene glycol and copper nanoparticles, which he suggested offered considerable potential for practical improvements in heat transfer applications. Ghalambaz et al. [3] reported that non-uniform magnetic fields can increase the rates of heat and mass transfer in MHD nanofluids inside a cavity. Rashid et al. [4] also found that nanoflow have the best behavior for thermal conductivity followed by lamina-shaped nanoparticles MHD applications in micro-nanotechnologies. Wahid et al. [5] studied hybrid nanofluids influenced by MHD and radiation case which presented significant improvement in heat transfer, whereas Swain [6] analyzed ternary-hybrid nanofluid problem considering viscous dissipation and Lorentz force for the convection flow of water with copper-alumina-silver nanoparticles. Ramzan et al. [7] investigated ternary hybrid nanofluids in kerosene oil and showed that their thermal conductivity can be significantly enhanced. Dash et al. [8] reported that copper kerosene nanofluids are superior compared to their water-based counterpart in terms of heat transfer enhancement. Bhandari et al. [9] optimized nanofluid flow over a shrinking surface, highlighting the impact of Biot and Grashof numbers on heat transfer. Kotha et al. [10] investigated bioconvection in MHD nanofluids with gyrotactic microorganisms, showing enhanced heat and mass transfer. Hussain et al. [11] compared heat transfer in water-based MHD nanofluids, finding Zn-water nanofluids superior to TiO_2-water nanofluids.

Studies of non-Newtonian fluids are critical in fluid mechanics due to their unique rheological characteristics, different from the predictable viscosities observed in Newtonian fluids [12]. Davis et al. [13] reported that these fluids exhibit intricate responses to external forces. Therefore, they are essential in numerous industrial and scientific fields, such as biomedical engineering and manufacturing. Second-grade fluids constitute an intriguing subclass of non-Newtonian fluids with a wide variability ([14]). Khan et al. [15] studied the time fractional second-grade MHD dusty fluid flow, highlighting the impact of heat and mass transfer rates on fluid dynamics. Entropy generation in Williamson fluid flow was investigated by Qayyum et al. [16], considering that thermal radiation and magnetic effects have a remarkable impact on entropy generation. Ahmed et al. [17] conducted a study on heat and mass dynamics within the MHD boundary layer flow of a second-grade fluid, discovering that chemical reactions and fluid oscillations reduced concentration levels. Anwar et al. [18] explored the transient MHD behavior of Oldroyd-B fluids, factoring in slip conditions and Newtonian heating effects to assess their influence on shear stress and heat distribution. Concurrently, Hayat et al. [19] conducted a study on the dual transport phenomena and entropy effects in MHD-driven second-grade nanofluid flows along a Riga plate, examining their contributions to thermal efficiency and entropy-related heat transformation. Khan et al. [20] studied how activation energy and complex heating and cooling processes impact the flow of Carreau nanofluids in environments influenced by radiation, focusing on how these factors affect speed and temperature changes. Das et al. [21] looked into how fluid flows with complex fluid properties, influenced by magnetic fields, chemical reactions, and heat transfer, contribute to irreversible energy loss. Chu et al. [22] examined how energy transfers in magnetically influenced nanofluids showing second-grade characteristics impact speed and temperature, highlighting significant effects from intense radiation. Tanveer et al. [23] studied electroosmosis in the peristaltic activity of MHD non-Newtonian fluid and illustrated the applications in micro-fabrication and chemical industries. Heat and mass transport in MHD flow of a non-Newtonian viscoelastic over a stretched magnetized surface were investigated by Aloliga et al. [24] and observed how induced magnetization was affecting heat transfer and flow behavior.

Boundary layer flows over-stretching sheets of various thicknesses are a topic of significant interest owing to their numerous applications in material processing and industrial manufacturing. The requirements for a fundamental understanding of fluid dynamics in flows of the boundary layer over continuously extending surfaces were laid down in the pioneering work of Sakiadis [25]. This represents a theoretical guideline for what has been experimentally demonstrated Tsou et al. [26]. Recent research has significantly progressed the description of boundary layer flows over stretching sheets including fluid dynamics, heat and mass transfer mechanisms as well as the influence of non-uniform sheet thickness. Hussain et al. [27] analyzed the entropy generation in MHD convection flow of hybrid nanofluids within a wavy enclosure, focusing on the impacts of heat generation and thermal radiation on thermal efficiency. Lin et al. [28] examined the behavior of fractional nanofluids in a porous medium, assessing the impact of magnetohydrodynamics and heat modifications on convective flow and heat transfer efficiency. Sharma et al. [29] conducted a numerical study of fractional boundary layer flow over a stretching sheet with variable thickness using a finite difference approach. Flow of a nanoliquid with gyrotactic microorganisms through the boundary layer over a stretching sheet was examined computationally by Hosseini et al. [30]. The nanofluid flow of variable thickness sheet with non-uniform stretching and porous velocities was examined by Alam et al. [31]. Rehman et al. [32] considered the influence of flow distribution on heat and mass transfer in MHD thin liquid film flow over an unsteady stretching sheet with mixed convection. Fatunmbi et al. [33] analyzed convective heat transfer in hydromagnetic micropolar fluid flow past an inclined nonlinear stretching sheet with variable thermo-physical properties.

This study extends the application of the Buongiorno model to explore the dynamic interactions of nanoparticle migration in a mixed convection second-grade fluid over a variable thickness stretching sheet. A comprehensive range of external influences including Joule heating, slip effects, thermal radiation, heat generation, and magnetohydrodynamic forces considered in the current assessment. To the authors' knowledge, applying the Buongiorno model to study nanoparticle migration in second-grade fluids over variable-thickness sheets with Joule heating and convective boundaries is unprecedented. The model was constructed based on flow assumptions, utilizing boundary layer approximations represented by partial differential equations. These equations were transformed into dimensionless form through appropriate scaling. Subsequently, the dimensionless equations were numerically solved using MATLAB software. The results of physical factors are deliberated through graphs as well as tables. This research not only broadens the theoretical framework but also enhances practical applications in industries where precise control of thermal and fluid dynamics is critical.

2 Methodology

This study investigates the steady incompressible flow of a mixed convection second-grade fluid over a variable thickness stretching sheet, modeled by $z = J(x+y+c)^{0.5(1-n)}$. Here, J acts as a geometric scaling factor that modulates the sheet's thickness. The parameter n influences surface configurations, as illustrated in Fig. 1. Analyzing the effects of Joule heating, slip conditions, thermal radiation, heat generation, and MHD forces, the study uses the Buongiorno model to examine nanoparticle behavior and the impact on heat and mass transfer efficiency. The governing equations derived from boundary layer approximations are dimensionless for numerical solution (see [34]):

$$\partial_x u + \partial_y v + \partial_z w = 0 \tag{1}$$

$$u\partial_x u + v\partial_y u + w\partial_z u = \nu\partial_{zz} u$$

$$+\alpha_{sg}\left(u\partial_{xzz}u+w\partial_{zzz}u-\partial_x u\partial_{zz}u-\partial_z u\partial_{zz}w-2\partial_z u\partial_{xz}u-2\partial_z w\partial_{zz}u\right)$$
$$-\frac{\sigma_{cond}B_{mag}^2}{\rho}u+g\left((T-T_\infty)\beta_T+(C-C_\infty)\beta_C\right) \tag{2}$$

$$u\partial_x v+v\partial_y v+w\partial_z v$$
$$=\nu\partial_{zz}v$$
$$+\alpha_{sg}\left(v\partial_{xzz}v+w\partial_{zzz}v-\partial_x v\partial_{zz}v-\partial_z v\partial_{zz}w-2\partial_z v\partial_{xz}v-2\partial_z w\partial_{zz}v\right)$$
$$-\frac{\sigma_{cond}B_{mag}^2}{\rho}v \tag{3}$$

$$u\partial_x T+v\partial_y T+w\partial_z T=\frac{k_f}{\rho c_{p_f}}\partial_{zz}T+\chi_{cp}\left(D_B\partial_z C\partial_z T+\frac{D_T}{T_\infty}(\partial_z T)^2\right)$$
$$-\frac{1}{\rho c_{p_f}}\partial_z q_{rad}+\frac{Q_{ga}}{\rho c_{p_f}}(T-T_\infty)+\frac{\sigma_{cond}B_{mag}^2}{\rho c_{p_f}}\left(u^2+v^2\right) \tag{4}$$

$$u\partial_x C+v\partial_y C+w\partial_z C=D_B\partial_{zz}C+\frac{D_T}{T_\infty}\partial_{zz}T \tag{5}$$

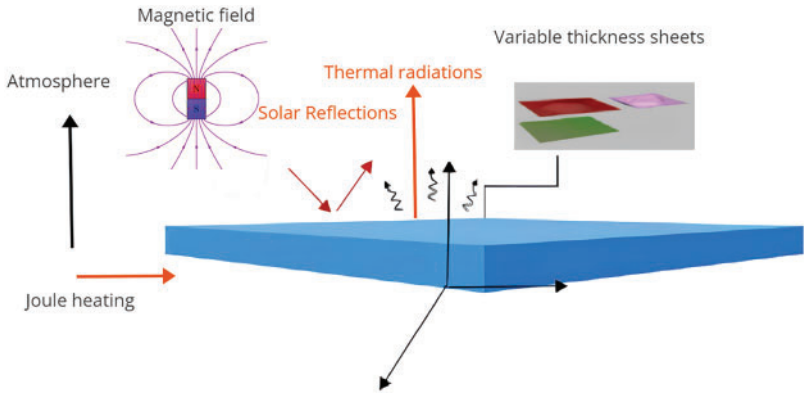

Figure 1: Schematic of flow geometry

The velocity conditions at the surface, where the thickness is variable

$$u-u_w-\epsilon_v\partial_z u=0,\quad v-v_w-\epsilon_v\partial_z v=0,\quad w=0 \tag{6}$$

whereas boundary conditions for concentration and temperature are detailed as follows:

$$-k_f\partial_z T=h_w(T_w-T),\quad -D_B\partial_z C=h_f(C_w-C) \tag{7}$$

at $z\to\infty$, the following asymptotic conditions hold:

$$u\to 0,\ v\to 0,\ T\to T_\infty,\ C\to C_\infty,\ \text{as}\ z\to\infty \tag{8}$$

The coefficients in the boundary conditions are defined as

$$\epsilon_v=\left(\frac{2-R_m}{R_M}\right)\xi_1\,(x+y+c)^{\frac{1-n}{2}},\ \xi_2=\frac{\xi_1}{\Pr},\ \xi_3=\frac{\xi_2}{\Pr},$$
$$u_w=U_0\,(x+y+c)^{\frac{1-n}{2}},\ v_w=U_0\,(x+y+c)^{\frac{1-n}{2}},$$

$$T_w = T_\infty + T_0\,(x+y+c)^{\frac{1-n}{2}},\ C_w = C_\infty + C_0\,(x+y+c)^{\frac{1-n}{2}}$$
$$Q_{ga} = Q_0\,(x+y+c)^{\frac{1-n}{2}},\ B_{mag} = B_0\,(x+y+c)^{\frac{n-1}{2}},\ Ec = Ec^*\,(x+y+c)^{\frac{1-n}{2}}$$

The equation for energy as (4) describes how the radiative heat flow q_{rad} is determined by applying the radiative transport equation [34,35].

$$q_{rad} = -\frac{4\sigma^4}{3k_1}\frac{\partial T^4}{\partial z^4} \tag{9}$$

Simply relying on the T^4 expansion around the temperature T_∞ is insufficient to explain radiative heat transfer fully. This overlooks some of these aspects. Therefore, we adjusted the energy equation to account for radiative heat flux accurately (see [34,35]).

$$u\partial_x T + v\partial_y T + w\partial_z T = \frac{k_f}{\rho c_{p_f}}\partial_{zz} T + \chi_{cp}\left(D_B\partial_z C\partial_z T + \frac{D_T}{T_\infty}(\partial_z T)^2\right)$$
$$u\partial_x T + v\partial_y T + w\partial_z T = \frac{k_f}{\rho c_{p_f}}\partial_{zz} T + \chi_{cp}\left(D_B\partial_z C\partial_z T + \frac{D_T}{T_\infty}(\partial_z T)^2\right)$$
$$+\frac{1}{\rho c_{p_f}}\partial_z\left(\frac{4\sigma^4}{3k_1^4}4T^3\partial_z T\right) + \frac{Q_{ga}}{\rho c_{p_f}}(T-T_\infty) + \frac{\sigma_{cond}B_{mag}^2}{\rho c_{p_f}}(u^2+v^2) \tag{10}$$

We have implemented transformations to simplify the mathematical formulation [34,35].

$$\zeta = \left[\frac{(n+1)\,U_0^2}{2\nu_f}\right]^{1/2}(x+y+c)^{(n-1)/2}\,z,\ \ \Psi = \left[\frac{2\nu_f U_0}{(n+1)^{1/2}}\right]^{1/2}(x+y+c)^{(n+1)/2}\,F(\zeta),$$
$$\Theta(\zeta) = \frac{T-T_\infty}{T_w-T_\infty},\ \Phi(\zeta) = \frac{C-C_\infty}{C_w-C_\infty},\ u = U_0\,(x+y+c)^n\,F'(\zeta),\ v = U_0\,(x+y+c)^n\,G'(\zeta),$$
$$w = -\left[\frac{2\nu_f U_0}{(n+1)^{\frac{1}{2}}}\right]^{\frac{1}{2}}(x+y+c)^{\frac{n-1}{2}}\left[\frac{n+1}{2}(F(\zeta)+G(\zeta)) + \frac{n-1}{2}\zeta\,(F'(\zeta)+G'(\zeta))\right] \tag{11}$$

Here, ζ represents the similarity variable, and Ψ refers to the stream function. By applying the transformation described in Eq. (11) to our set of equations and the specified boundary conditions, we establish the corresponding nonlinear ordinary differential equations (ODEs).

$$\left(\frac{n+1}{2}\right)F^{(4)} + \beta_1\left[2n\,(n+1)\,G' + (n+1)\,(3n-1)\,F'\right]F''' - \frac{1}{2}\left[(G+F)\frac{n+1}{2} + \left(n^2-1\right)\eta G'\right]$$
$$-MF\prime + (\lambda_1\theta+\lambda_2) - \left[nF'G' + nF''^2 - \frac{n+1}{2}(F+G)\,F'''\right] = 0 \tag{12}$$

$$\left(\frac{n+1}{2}\right)G^{(4)} + \beta_1\left[2n(n+1)F' + (n+1)(3n-1)G'\right]G'''$$
$$-\frac{1}{2}\left[(F+G)^{\frac{n+1}{2}} + \left(n^2-1\right)\eta F'''\right]G^{(4)} - MG'$$

$$-\left[nG'F' + nG''^2 - \frac{n+1}{2}(G+F)G'''\right] = 0 \tag{13}$$

$$Pr\left(\frac{1-n}{n+1}\right)(F'+G')\,\Theta - (F+G)\,\Theta' + \frac{2}{n+1}I_H\Theta + N_{bm}\Theta' + N_{tp}\Theta'^2 + \frac{2}{n+1}Ec\left(F'^2+G'^2\right) + \left(1+\frac{4}{3}\Pi_{rad}\right)\Theta'' = 0 \tag{14}$$

$$\Phi'' + Sc\left((F+G)\,\Phi' - \frac{1-n}{n+1}(F'+G')\,\Phi\right) + \frac{N_{tp}}{N_{bm}}\Theta'' = 0 \tag{15}$$

The corresponding boundary conditions are

$$F(\zeta) = \lambda\left(\frac{1-n}{1+n}\right)(1+\tau_1 F''(\zeta)),\ F'(\zeta) = 1+\tau_1 F''(\zeta),$$

$$\Theta'(\zeta) = -\gamma_1(1-\Theta(\zeta)),\ G(\zeta) = \lambda\left(\frac{1-n}{1+n}\right)(1+\tau_1 G''(\zeta)),$$

$$G'(\zeta) = 1+\tau_1 G''(\zeta),\ \Phi'(\zeta) = -\gamma_2(1-\Phi(\zeta)),\ \text{at } \zeta = \lambda,$$

$$F'(\infty) = 0,\ G'(\infty) = 0,\ \Theta(\infty) = 0,\ \Phi(\infty) = 0 \tag{16}$$

To make it easier to analyze the intricate differential Eqs. (12)–(15), and related boundary conditions (16) that were originally established across the range $[\lambda, \infty)$ are now redefined in a different domain $[0, \infty)$. This change simplifies the procedure by moving the variable making it simpler and more organized to solve these equations.

The transformed differential equations are given by

$$\left(\frac{n+1}{2}\right)f^{(4)} + \beta_1[2n(n+1)g' + (n+1)(3n-1)f']f''' - \frac{1}{2}\left[(g+f)^{\frac{n+1}{2}} + \left(n^2-1\right)\eta g''''\right]f^{(4)} - Mf' + (\lambda_1\theta+\lambda_2) - \left[nf'g' + nf''^2 - \frac{n+1}{2}(f+g)f'''\right] = 0 \tag{17}$$

$$\left(\frac{n+1}{2}\right)g^{(4)} + \beta_1[2n(n+1)f' + (n+1)(3n-1)g']g''' - \frac{1}{2}\left[(f+g)^{\frac{n+1}{2}} + \left(n^2-1\right)\eta f''''\right]g^{(4)} - Mg' - \left[ng'f' + ng''^2 - \frac{n+1}{2}(g+f)g'''\right] = 0 \tag{18}$$

$$Pr\left(\frac{1-n}{n+1}\right)(f'+g')\,\theta - (f+g)\,\theta' + \frac{2}{n+1}I_H\theta + N_{bm}\theta' + N_{tp}\theta'^2 + \frac{2}{n+1}Ec(f'^2 + g'^2)\left(1+\frac{4}{3}\Pi_{rad}\right)\theta'' = 0 \tag{19}$$

$$\phi'' + Sc\left((f+g)\,\phi' - \frac{1-n}{n+1}\,(f'+g')\,\phi\right) + \frac{N_{tp}}{N_{bm}}\theta'' = 0 \tag{20}$$

The corresponding boundary conditions at the transformed domain are:

$$\begin{aligned} &f(0) = \lambda\left(\frac{1-n}{1+n}\right) + \tau_1 f''(0), \quad f'(\infty) = 0, \quad f'(0) = 1 + \tau_1 f''(0), \theta(\infty) = 0, \\ &\theta'(0) = -\gamma_1(1-\theta(0)), \quad g'(\infty) = 0, \quad g(0) = \lambda\left(\frac{1-n}{1+n}\right) + \tau_1 g''(0), \quad \phi(\infty) = 0, \\ &g'(0) = 1 + \tau_1 g''(0), \quad \phi(0) = -\gamma_2(1-\phi(0)) \end{aligned} \tag{21}$$

The following parameters are introduced to thoroughly analyzed the behavior of flow and heat and mass transfer effects in the systems:

$$\begin{aligned} &M = \frac{\sigma_{cond} B_0^2}{\rho_f U_0}, \quad \beta_1 = \frac{u_w \alpha_{sec}}{\nu}, \quad \Pr = \frac{\mu_f c_{p_f}}{k_f}, \quad \Pi_{rad} = \frac{4\sigma^4 T_\infty^3}{k_f k_1^*}, \quad N_{bm} = \frac{\chi_{cp} D_B (C_w - C_\infty)}{\nu_f}, \\ &N_{tp} = \frac{\chi_{cp} D_T (T_w - T_\infty)}{\nu_f T_\infty}, Sc = \frac{\nu_f}{D_B}, \quad \tau_1 = \frac{2-R_m}{R_m}\xi_1 (x+y+c)^{0.5(1-n)}, \\ &\gamma_1 = \frac{h_w}{k_f}\left(\frac{2\nu_f}{(n+1)\,u_w^2}\right)^{0.5}, \lambda = J\left(\frac{(n+1)\,U_0^2}{2\nu_f}\right)^{0.5}(x+y+c)^{0.5(n-1)}, \quad \gamma_2 = \frac{h_f}{D_B}\left(\frac{2\nu_f}{(n+1)\,u_w^2}\right)^{0.5} \end{aligned} \tag{22}$$

Frictional resistance coefficient, mass transfer coefficient, and heat transfer coefficient are discussed below to determine the numerical solutions

$$\begin{aligned} \mathrm{Re}_x^{\frac{1}{2}} C_{Fx} = 2\Bigg(\Bigg(\frac{n+1}{2}\Bigg)^{\frac{1}{2}} &(f'''(0) \\ &+ 2\beta_1\Big[g'(0)^2 f''(0) + (f'(0)+g'(0))^2 + 2nf'(0)f''(0) \\ &+ nf'(0)^2 f''(0) - \frac{n+1}{2}(f(0)+g(0))f'''(0)\Big]\Bigg)\Bigg), \end{aligned}$$

$$\begin{aligned} \mathrm{Re}_y^{\frac{1}{2}} C_{Fy} = 2\Bigg(\Bigg(\frac{n+1}{2}\Bigg)^{\frac{1}{2}} &(g'''(0) \\ &+ 2\beta_1\left[f'(0)^2 g''(0) + (g'(0)+f'(0))^2 + 2ng'(0)g''(0)\right. \\ &\left. + ng'(0)^2 g''(0) - \frac{n+1}{2}(g(0)+f(0))g'''(0)\right]\Bigg)\Bigg), \end{aligned}$$

$$Nu_x Re_x^{-\frac{1}{2}} = -\left(1+\frac{4}{3}\Pi_{rad}\right)\left(\frac{1+n}{2}\right)^{\frac{1}{2}}\theta'(0), Sh_x Re_x^{-\frac{1}{2}} = -\left(\frac{1+n}{2}\right)^{\frac{1}{2}}\phi'(0),$$

$$\mathrm{Re}_x = \frac{u_w(x)\,(x+y+c)}{\nu_f}$$

3 Numerical Solution Approach

The dimensionless system, represented by ordinary differential equations (ODEs), is elucidated using numerical techniques. This method transforms higher-order nonlinear differential equations into first-order ones. The process is outlined below (refer to Fig. 2).

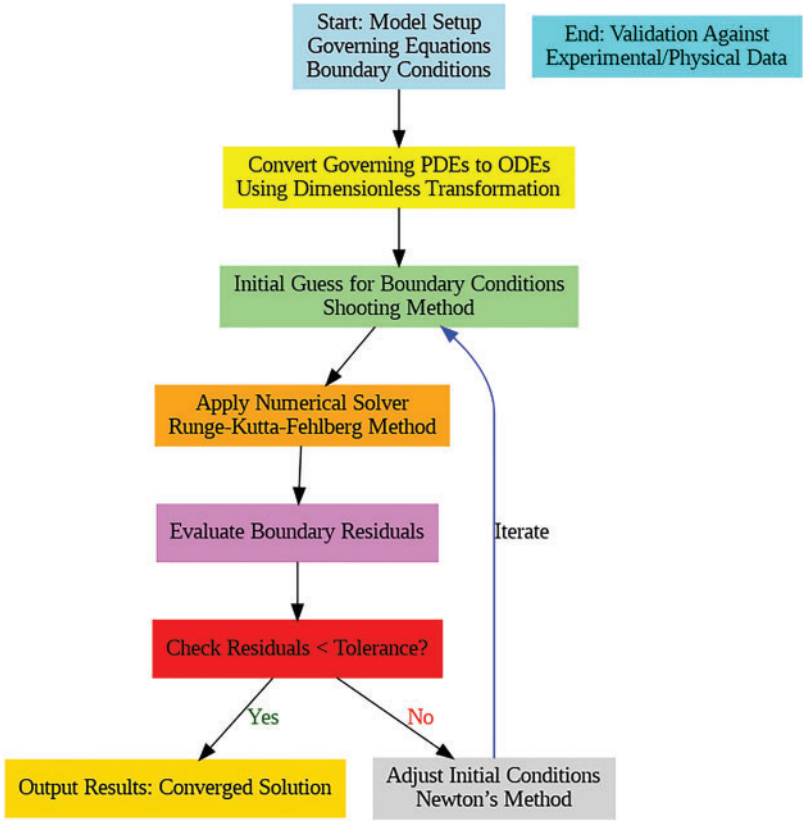

Figure 2: Schematic representation of the computational algorithm

Let's introduce these variables: - $u_1 = f$, $u_2 = f'$, $u_3 = f''$, $u_4 = f'''$ - $v_1 = g$, $v_2 = g'$, $v_3 = g''$, $v_4 = g'''$ - $w_1 = \theta$, $w_2 = \theta'$ - $z_1 = \phi$, $z_2 = \phi'$

$$u_{1'} = u_2,$$

$$u_{2'} = u_3,$$

$$u_{3'} = u_4,$$

$$u_{4'} = \left(\frac{2}{n+1}\right)\left(\begin{array}{l} -\beta_1\left[2n\left(n+1\right)v_2 + \left(n+1\right)\left(3n-1\right)u_2\right]u_4 + \frac{1}{2}\left[\left(v_1+u_1\right)\frac{n+1}{2} + \left(n^2-1\right)\eta v_2\right]u_4 \\ +Mu_2 - \left(\lambda_1 w_1 + \lambda_2\right) + \left[nu_2v_2 + nu_3^2 - \frac{n+1}{2}\left(u_1+v_1\right)u_4\right]\end{array}\right), \tag{23}$$

$$v_{1'} = v_2,$$

$$v_{2'} = v_3,$$

$$v_{3'} = v_4,$$

$$v_{4'} = \left(\frac{2}{n+1}\right)\Bigg(\Bigg(-\beta_1\left[2n(n+1)u_2 + (n+1)(3n-1)v_2\right]v_4 + \frac{1}{2}\left[(u_1+v_1)^{\frac{n+1}{2}} + (n^2-1)\eta u_2\right]v_4 + Mv_2 - (\lambda_1 w_1 + \lambda_2) + \left[nv_2u_2 + nv_3^2 - \frac{n+1}{2}(v_1+u_1)\,v_4\right]\Bigg)\Bigg) \tag{24}$$

$$w_{1'} = w_2,$$

$$w_{2'} = -\frac{1}{1+\frac{4}{3}\Pi_{rad}}\left(\Pr\frac{1-n}{n+1}(u_2+v_2)\,w_1 - (u_1+v_1)\,w_2 - \frac{2}{n+1}I_H w_1 - N_{bm}w_2 - N_{tp}w_2^2 - \frac{2}{n+1}Ec(u_2^2+v_2^2)\right) \tag{25}$$

$$z_{1'} = z_2,$$

$$z_{2'} = -\frac{1}{\mathrm{Sc}}\left((u_1+v_1)\,z_2 - \frac{1-n}{n+1}(u_2+v_2)\,z_1 - \frac{N_{tp}}{N_{bm}}w_{2'}\right) \tag{26}$$

With boundary conditions

$$\begin{aligned} &u_1(0) = \lambda\left(\frac{1-n}{1+n}\right) + \tau_1 u_3(0), \qquad u_2(\infty) = 0, u_2(0) = 1 + \tau_1 u_3(0), w_1(\infty) = 0, \\ &w_2(0) = -\gamma_1(1 - w_1(0)), \qquad v_2(\infty) = 0, v_1(0) = \lambda\left(\frac{1-n}{1+n}\right) + \tau_1 v_3(0), z_1(\infty) = 0, \\ &v_2(0) = 1 + \tau_1 v_3(0), z_2(0) = -\gamma_2(1 - z_1(0)) \end{aligned} \tag{27}$$

4 Results and Discussion

This investigation explores the complex behavior of nanofluid flow over a surface that is stretched in a manner affected by different factors. It examines the interaction between the nanofluid and irregular surface and the influence of external forces, such as magnetohydrodynamics (MHD) and thermophoresis. This section analyzes the impact of different critical parameters on the velocity, temperature, and concentration profiles. These parameters include the parameter M velocity power index parameter n second-grade fluid parameter β_1 and several thermal- and concentration-related parameters. Understanding these variables is crucial for comprehending the complexities of nanofluid behavior and its potential applications in engineering and technology. Fig. 3 illustrates how changes in parameter M affect both the stretch-induced velocity profile f' and the cross-stretch velocity profile g'. As the strength of the field increases, it causes a Lorentz force to act against the flow, resulting in a decrease in f'. Similarly, in the perpendicular direction (along g', the cross-flow is also inhibited by the magnetic forces, leading to a decrease in the velocity gradient perpendicular to the primary flow. Fig. 4 shows how the velocity slip parameter τ_1 affects both f' and g'. As τ_1 increased, these velocity

profiles decreased, indicating a slip at the boundary. A higher value of τ_1 signifies an increased slip at the boundary, enabling fluid flow with reduced resistance and consequently resulting in velocity gradients for both f' and g'.

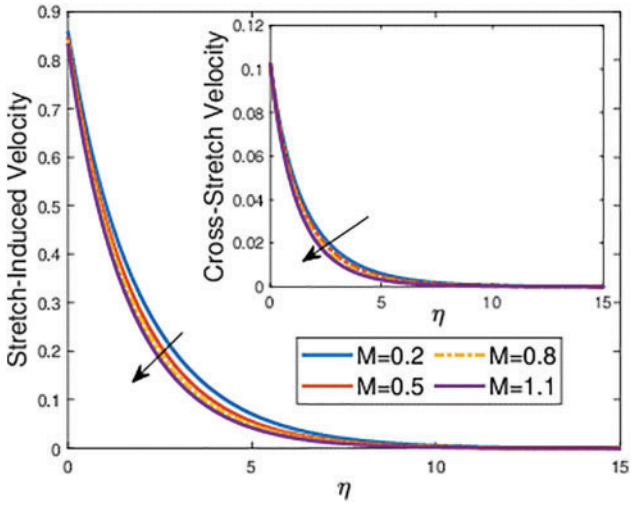

Figure 3: Effects of the magnetic parameter $\boldsymbol{M}$ on $\boldsymbol{f'}$ and $\boldsymbol{g'}$

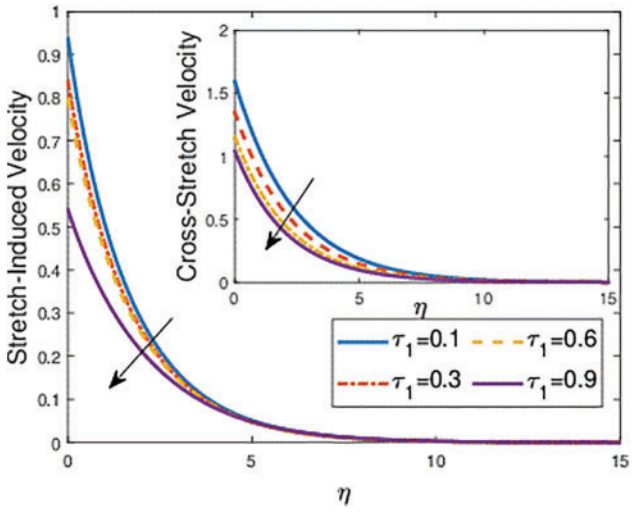

Figure 4: Effects of the velocity slip parameter $\boldsymbol{\tau_1}$ on $\boldsymbol{f'}$ and $\boldsymbol{g'}$

The impact of the velocity index parameter, denoted by n on the velocity profiles caused by stretching, represented by f' and g' is depicted in Fig. 5. This parameter demonstrates that the behavior of the velocity profile follows a power-law pattern. As the value of n increases, both f' and g' exhibit a trend indicating a significant variation in the velocity near the surface. With an increasing power index parameter, the velocity gradients in both profiles became more pronounced, accelerating the flow from the surface. Fig. 6 illustrates how the second-grade fluid parameter, β_1, affects both f' and g'. As β_1 increases, we consistently observe an increase in these velocity profiles. This trend can be physically justified by the fluid's enhanced elasticity which allows it to respond more dynamically to changes in

flow and boundary interactions. The increase in β_1 amplifies the fluid's ability to store and release elastic energy, leading to higher velocity gradients f' and g'.

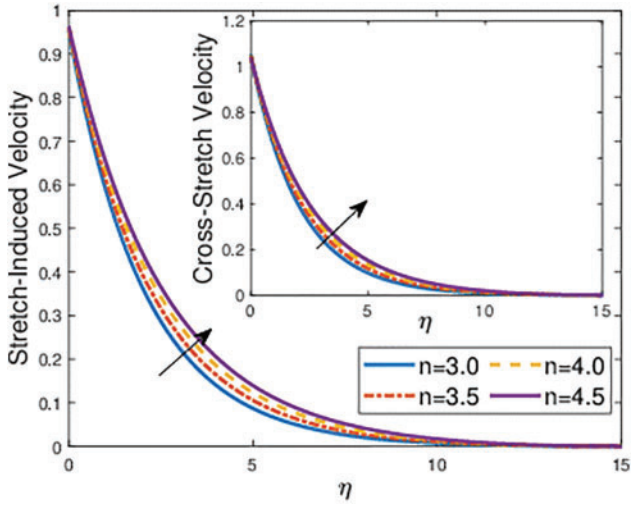

Figure 5: Effects of the velocity power index parameter n on f' and g'

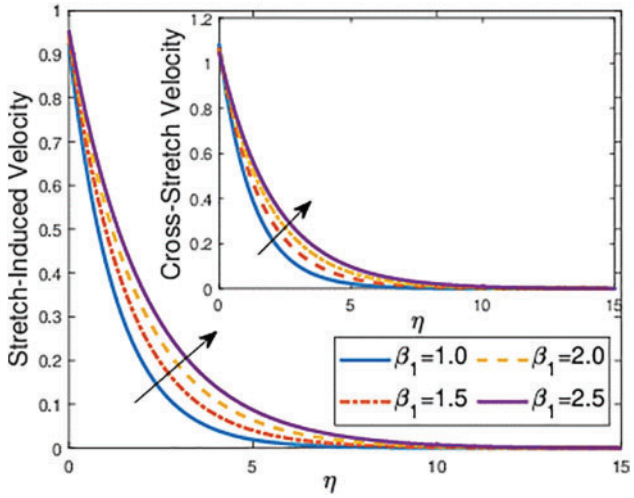

Figure 6: Effects of the second grade fluid parameter β_1 on f' and g'

Fig. 7 shows the effects of increasing the thermal Grashof number λ_1 on the velocity gradients f' and g'. As λ_1 increases, there is a clear increase in f', indicating that the buoyancy-driven flow becomes more pronounced. This enhancement in f' suggests that the upward buoyant force, which aids in driving the fluid flow against gravitational pull, is strengthened with higher λ_1, thereby accelerating the fluid more significantly in the primary flow direction. Conversely, while there is also an increase in g', its change is minimal, particularly in the curved regions of the flow, suggesting that the cross-flow is less affected by buoyancy. The impact of the Eckert number Ec on the temperature profile θ is exhibited in Fig. 8. An increase in Ec leads to a noticeable increase in the temperature profile θ. This trend highlights the conversion of kinetic energy into thermal energy through viscous dissipation,

underscoring a direct relationship between mechanical energy dissipation and temperature increase in the fluid.

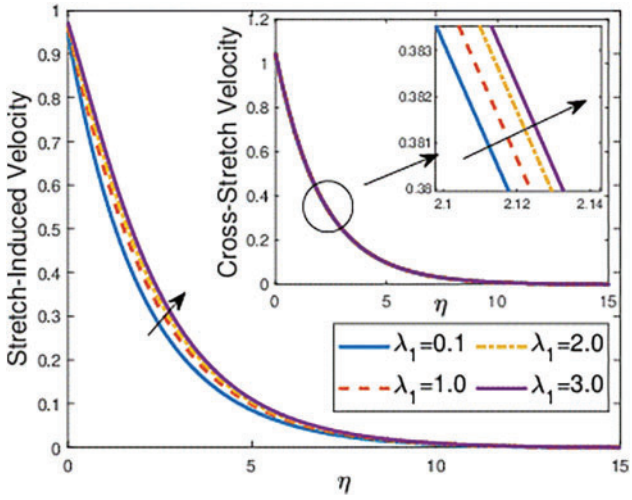

Figure 7: Effects of the thermal Grashof number $\boldsymbol{\lambda_1}$ on $\boldsymbol{f'}$ and $\boldsymbol{g'}$

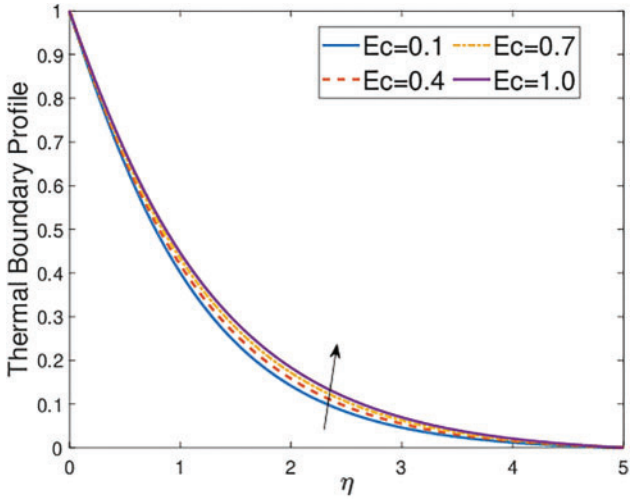

Figure 8: Effects of the Eckert number $\boldsymbol{Ec}$ on $\boldsymbol{\theta}$

The Fig. 9 demonstrates how the thermophoresis parameter N_{tp} and the Brownian motion parameter N_{bm} impact the thermal boundary profile θ. As the value of N_{tp} increases, the value of θ. This is because the stronger thermophoretic force pushes the nanoparticles away from the surface, resulting in a wider thermal boundary layer. Similarly, when N_{bm} is higher, the energy transfer between the particles and fluid increases, resulting in a boundary layer. Fig. 10 shows how an increase in the thermal Biot number, γ_1, affects the temperature profile θ. Higher γ_1 indicates increased internal resistance to heat conduction compared to external convective transfer, resulting in a pronounced temperature gradient. This leads to a thicker thermal boundary layer as the surface quickly equilibrates with the environment, while the interior heats up more slowly. The effect is a more distinct temperature variation across the fluid, highlighting the importance of γ_1 in thermal management.

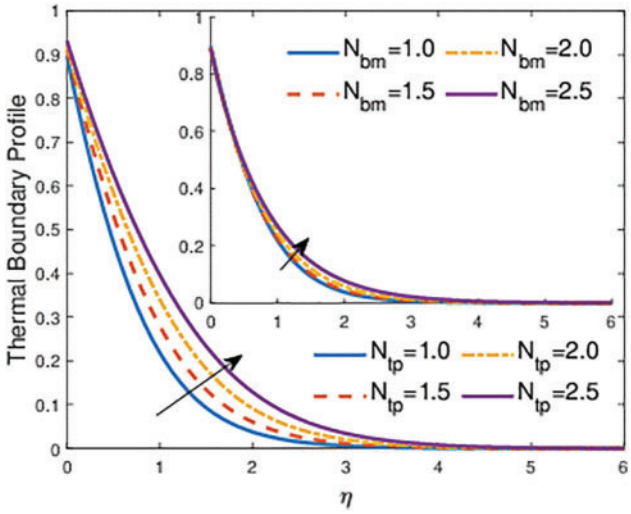

Figure 9: Effects of the thermophoresis parameter N_{tp} and the Brownian motion parameter N_{bm} on θ

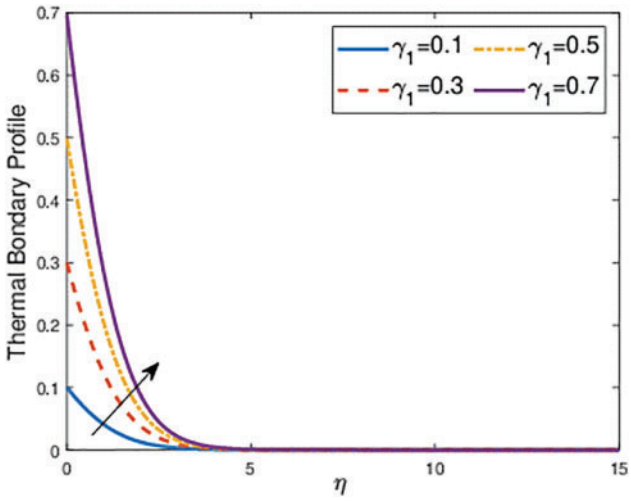

Figure 10: Effects of the thermal Biot number γ_1 on θ

In Fig. 11, we observe the impact of the radiation parameter Π_{rad} on the layer. The thermal boundary layer became more noticeable as the value of Π_{rad} increased. This is because of the increased radiative heat transfer, which allows energy dissipation away from the boundary layer and creates a wider temperature difference. As shown in Fig. 12, we can see how the heat-generation parameter I_H affects the profile θ of the boundary layer. The growth of this layer was caused by the thermal energy generated within the fluid owing to the increase in I_H. The internal heat generation within the enhanced heat distribution resulted in a more extensive thermal boundary layer. This behavior highlights the effect of internal heat sources on the flow properties.

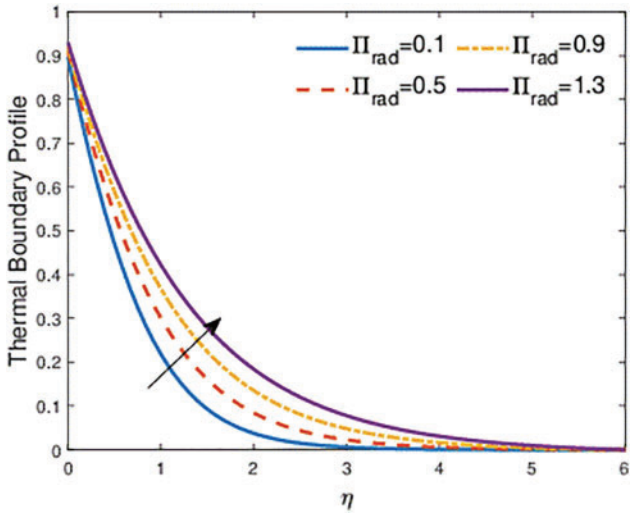

Figure 11: Effects of the radiation parameter $\boldsymbol{\Pi}_{rad}$ on $\boldsymbol{\theta}$

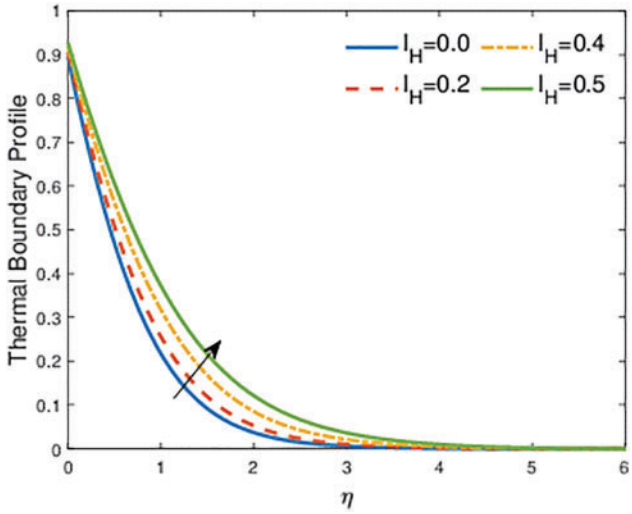

Figure 12: Effects of the internal heat generation parameter $\boldsymbol{I}_H$ on $\boldsymbol{\theta}$

Fig. 13 shows how changes in N_{tp} and N_{bm} affect the behavior of the concentration boundary profile ϕ. When the thermophoresis parameter N_{tp} increases, it also leads to an increase in ϕ, indicating that the particles move intensely from the areas to colder ones. This occurs because, as N_{tp} increases, the thermophoretic force becomes more significant, causing the nanoparticles to be displaced from the surface, resulting in a concentration within the boundary layer. On the contrary, when we increased the motion parameter N_{bm} we observed a reduction in the value of ϕ. This suggests that increased motion, which refers to particle movement, leads to a more even distribution of the NPs and decreases the concentration gradient near the surface. Fig. 14 demonstrates how an increase in the concentration Biot number, γ_2, influences the concentration profile. A higher γ_2 suggests greater internal resistance to diffusion compared to the surface mass transfer, resulting in a steeper concentration gradient at the boundary. This differential leads to a more defined concentration boundary layer, as the surface adjusts

to environmental changes more rapidly than the interior. Consequently, there is a more pronounced variation in concentration throughout the fluid, underscoring the significance of γ_2 in managing diffusion processes.

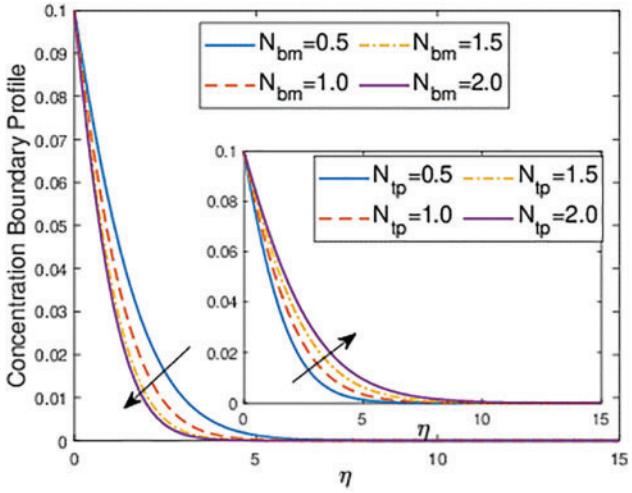

Figure 13: Effects of the thermophoresis parameter N_{tp} and Brownian motion parameter N_{bm} on ϕ

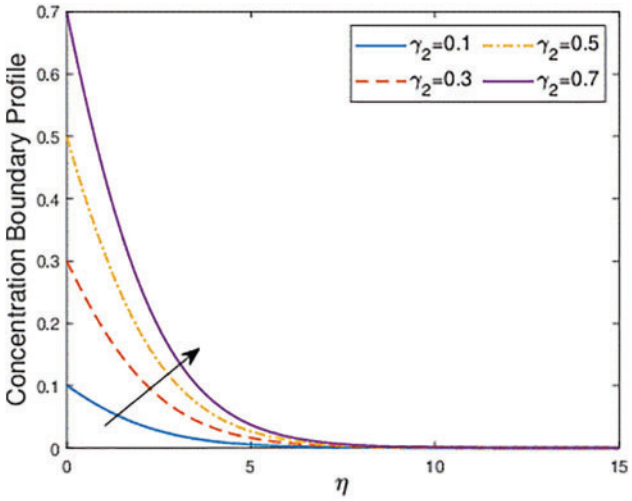

Figure 14: Effect of the concentration Biot number γ_2 on ϕ

Our study examines the influence of various physical parameters on skin friction and heat and mass transfer in fluid flow, as detailed in Tables 1 and 2. Table 1 highlights the effects of parameters such as τ_1, M, γ_1, and λ on the skin friction coefficients CFx. It is evident that even minor adjustments in the velocity slip parameter τ_1 can cause significant changes in skin friction. For example, increasing M from 0.22 to 0.88 results in a CFx decrease of 37.5%, indicating a strong influence of magnetic fields on friction. Moreover, changes in the wall thickness parameter λ from 0.33 to 0.99 lead to a decrease in CFx by 1.1%.

Table 1: Numerical results of physical parameters for skin friction

τ_1	M	γ_1	λ	CFx
0.1	0.42	0.62	0.72	−2.2950
0.2				−2.0250
0.3				−1.8150
0.4				−1.6450
	0.22			−1.7600
	0.44			−2.0300
	0.66			−2.2400
	0.88			−2.4200
		0.22		−2.0305
		0.44		−1.7350
		0.66		−1.5400
		0.88		−1.4050
			0.33	−1.6400
			0.55	−1.6505
			0.77	−1.6575
			0.99	−1.6585

Table 2: Effects of parameter variations on nusselt and sherwood numbers

N_t	N_b	τ_2 / Sc	n	Nu	Sh
1	1	0.1/0.5	0.39	0.72163	0.44131
1.5				0.61465	0.53352
2				0.53404	0.59985
2.5	1			0.47286	0.64677
	1.5			0.54185	0.54774
	2			0.61799	0.48794
	2.5	0.1/0.5		0.70025	0.44442
		0.2/0.7		0.6762	0.54770
		0.3/0.9		0.65176	0.62999
		0.4/1.1	0.39	0.62475	0.68888
			0.41	0.63374	0.69879
			0.43	0.64273	0.70870
			0.45	0.65172	0.71861

Table 2 analyzes the correlation between parameters N_{tp}, N_{bm}, γ_1, Sc, and n with the heat and mass transfer characteristics measured by Nusselt (Nu) and Sherwood (Sh) numbers. The Brownian motion parameter N_{bm} and the thermophoresis parameter N_{tp} notably increase both Nu and Sh, with Nu seeing increases up to 14.6% and Sh up to 23.2%. Increases in the Biot number (γ_1) for heat transfer, reflecting

improved heat transfer efficiency at the surface relative to the interior. Similarly, a rise in the thermal Biot number (γ_2) for mass transfer, enhances the Sherwood number (Sh), indicating more effective convective mass transfer compared to diffusion. Similarly, an increase in the Schmidt number (Sc) enhances the mass transfer rate as indicated by a rise in Sh, with percentage increases reflecting the direct correlation with Sc. The velocity power index (n) also significantly affects these transfer rates, with increases in n resulting in corresponding rises in both Nu and Sh by approximately 1.4%.

In Tables 3 and 4, we present a comparison of our study findings with the results from previous research by Nadeem et al. [34], Kebede et al. [36], and Pop et al. [37]. These comparisons specifically focus on the behaviors of $f''(0)$, $\theta'(0)$, and $\phi'(0)$ for different values of n and Pr. Our results are closely aligned with those reported in the literature, reinforcing the validity and precision of our computational approach.

Table 3: Comparison of $\boldsymbol{f''(0)}$, $\boldsymbol{-\theta'(0)}$, and $\boldsymbol{-\phi'(0)}$ for varying $\boldsymbol{n}$

n	Kebede et al. [36]			Pop et al. [37]			Present study		
0	0.4688	0.4228	0.2326	0.4649	0.8769	0.4690	0.4638	0.4630	0.2339
0.1	0.8023	0.5402	0.2669	0.8021	0.8027	0.5510	0.8077	0.5536	0.2656
0.5	1.0389	0.6369	0.2822	1.0389	1.0391	0.6371	1.0397	0.6375	0.2894
1	1.2326	0.7202	0.3063	1.2326	1.1279	1.2330	1.2368	0.7250	0.3011
5	1.5503	0.8648	0.3517				1.5568	0.8798	0.3531

Table 4: Comparison of heat transfer coefficient for various values of $\boldsymbol{Pr}$

Pr	Nadeem et al. [34]	Present analysis
0.50	0.3258130	0.327898
1.00	0.5267410	0.528773
1.50	0.6918720	0.694984
2.00	0.8362780	0.838559

5 Conclusion

This research applies the Buongiorno model to investigate the behavior of nanoparticles in a mixed convection second-grade fluid flowing over a variable thickness stretching sheet. Key features such as Joule heating, slip effects, thermal radiation, heat generation, and magnetohydrodynamic forces are considered. The main findings of this study are as follows:

- Increasing Π_{rad} enhances the temperature profile, expanding the thermal boundary layer.
- Increasing the thermal Biot number enhances the temperature gradient at the boundary, while a rise in the concentration Biot number sharpens the concentration gradient at the boundary.
- Higher second-grade fluid parameters increase velocity profiles due to enhanced fluid elasticity.
- An increase in the velocity slip parameter reduces velocity gradients by lowering boundary resistance.

- Nusselt and Sherwood numbers increase by up to 14.6% and 23.2%, respectively, due to higher Brownian motion and thermophoresis parameters.
- Skin friction coefficients decrease by 37.5% with increasing magnetic field strength.

Investigating different fluid models such as Oldroyd-B and Sisko fluids on complex surfaces could provide further insights into non-Newtonian behaviors under stretching and magnetic influences. This research could enhance applications in industries that demand precise fluid dynamics control.

Acknowledgement: The authors would like to express their gratitude to the reviewers for their insightful and constructive comments, which have significantly contributed to enhancing the quality of this article according to the journal's standards.

Funding Statement: The authors received no specific funding for this study.

Author Contributions: The authors confirm their contributions to the paper as follows: study conception and design: Muhammad Shoaib Anwar; analysis and interpretation of results: Mumtaz Khan; draft manuscript preparation: Muhammad Shoaib Anwar, Mumtaz Khan. Mudassar Imran and Amer Rasheed contributed to addressing reviewer comments and the preparation of the revised manuscript. All authors reviewed the results and approved the final version of the manuscript.

Availability of Data and Materials: All data generated or analyzed during this study are included within this article.

Ethics Approval: This study did not involve human or animal subjects and, as such, ethical approval was not required.

Conflicts of Interest: The authors declare that they have no conflicts of interest to report regarding the present study.

References

1. Choi SUS, Eastman JA. Enhancing thermal conductivity of fluids with nanoparticles. ASME Fed. 1995;231:99–105.
2. Eastman JA, Choi SUS, Li S, Yu W, Thompson LJ. Anomalously increased effective thermal conductivities of ethylene glycol-based nanofluids containing copper nanoparticles. Appl Phys Lett. 2001;78:718–20. doi:10.1063/1.1341218.
3. Ghalambaz M, Sabour M, Sazgara S, Pop I, Trambitas R. Insight into the dynamics of ferrohydrodynamic (FHD) and magnetohydrodynamic (MHD) nanofluids inside a hexagonal cavity in the presence of a non-uniform magnetic field. J Magn Magn Mater. 2020;497:166024. doi:10.1016/j.jmmm.2019.166024.
4. Rashid U, Liang H, Baleanu D, Iqbal A, Abbas M. Shape effect of nanosize particles on magnetohydrodynamic nanofluid flow and heat transfer over a stretching sheet with entropy generation. Entropy. 2020;22(10):1171. doi:10.3390/e22101171.
5. Wahid NS, Arifin N, Khashi'ie N, Pop I, Bachok N, Hafidzuddin E. MHD hybrid nanofluid flow with convective heat transfer over a permeable stretching/shrinking surface with radiation. Int J Numer Methods Heat Fluid Flow. 2021;32(5). doi:10.1108/HFF-04-2021-0263.
6. Swain B. Dynamics of ternary-hybrid nanofluid of water conveying copper, alumina and silver nanoparticles when entropy generation, viscous dissipation, Lorentz force are significant. ZAMM. 2023;103(9):e202200254. doi:10.1002/zamm.202200254.

7. Ramzan M, Dawar A, Saeed A, Kumam P, Sitthithakerngkiet K, Lone S. Analysis of the partially ionized kerosene oil-based ternary nanofluid flow over a convectively heated rotating surface. Open Phys. 2022;20:507–25. doi:10.1515/phys-2022-0055.
8. Dash R, Mishra S, Pattnaik PK. Influence of radiative heat energy on the MHD flow of Cu-kerosene nanofluid over a vertical plate: laplace transform technique. Biointerface Res Appl Chem. 2021;12(5):6234–51. doi:10.33263/BRIAC125.62346251.
9. Bhandari A, Pannala R. Optimization of heat transfer properties of nanofluid flow over a shrinking surface through mathematical modeling. Int J Appl Mech Eng. 2020;25(1):40–56. doi:10.2478/ijame-2020-0019.
10. Kotha G, Kolipaula VR, Rao MVS, Penki S, Chamkha AJ. Internal heat generation on bioconvection of an MHD nanofluid flow due to gyrotactic microorganisms. Eur Phys J Plus. 2020;135(6). doi:10.1140/epjp/s13360-020-00606-2.
11. Hussain A, Arshad M, Rehman A, Hassan A, Elagan S, Ahmad H et al. Three-dimensional water-based magneto-hydrodynamic rotating nanofluid flow over a linear extending sheet and heat transport analysis: a numerical approach. Energies. 2021;14(16):5133. doi:10.3390/en14165133.
12. Smith AB, Johnson CD. Advanced rheology of non-Newtonian fluids. J Fluid Mech. 2018;123:45–67.
13. Davis LE, Lee MJ. Industrial applications of non-Newtonian fluids. Eng Appl. 2017;15(2):89–102.
14. Green P, Thompson K. Characteristics of Second-Grade Fluids. Rheol Today. 2021;20(4):210–25.
15. Khan Z, Ali F, Haq S, Khan I. A time fractional second-grade magnetohydrodynamic dusty fluid flow model with variable conditions: application of Fick's and Fourier's laws. Front Phys. 2022;10:1006893. doi:10.3389/fphy.2022.1006893.
16. Qayyum S, Khan M, Masood F, Chu Y, Kadry S, Nazeer M. Interpretation of entropy generation in Williamson fluid flow with nonlinear thermal radiation and first-order velocity slip. Math Meth Appl Sci. 2020;44:7756–65. doi:10.1002/mma.6735.
17. Ahmed NA, Krishna MV, Aljohani A. Heat and mass transfer in MHD boundary layer flow of a second-grade fluid past an infinite vertical permeable surface. Heat Transf. 2021;50:6022–42. doi:10.1002/htj.22160.
18. Anwar T, Kumam P, Asifa, Thounthong P, Muhammad S, Duraihem FZ. Generalized thermal investigation of unsteady MHD flow of Oldroyd-B fluid with slip effects and Newtonian heating; a Caputo-Fabrizio fractional model. Alex Eng J. 2021;61(3):2188–202. doi:10.1016/j.aej.2021.06.090.
19. Hayat T, Shah F, Alseadi A. Cattaneo-Christov double diffusions and entropy generation in MHD second grade nanofluid flow by a Riga wall. Int Commun Heat Mass Transf. 2020;119:104824. doi:10.1016/j.icheatmasstransfer.2020.104824.
20. Khan M, Alzahrani F. Dynamics of activation energy and nonlinear mixed convection in Darcy-Forchheimer radiated flow of Carreau nanofluid near stagnation point region. J Therm Sci Eng Appl. 2021;13. doi:10.1115/1.4049434.
21. Das S, Sarkar S, Jana R. Assessment of irreversible losses of non-Newtonian nanofluid flow underlying hall current, chemical reaction and thermal radiation. World J Eng. 2020;18(2):228–50. doi:10.1108/WJE-07-2020-0266.
22. Chu Y, Shah F, Khan M, Kadry S, Abdelmalek Z, Khan W. Cattaneo-Christov double diffusions (CCDD) in entropy optimized magnetized second grade nanofluid with variable thermal conductivity and mass diffusivity. J Mater Res Technol. 2020;9:13977–87. doi:10.1016/j.jmrt.2020.09.101.
23. Tanveer A, Mahmood S, Hayat T, Alsaedi A. On electroosmosis in peristaltic activity of MHD non-Newtonian fluid. Alex Eng J. 2021;60:3369–77. doi:10.1016/j.aej.2020.12.051.
24. Aloliga G, Seini IY, Musah R. On MHD flow of non-Newtonian viscoelastic fluid over a stretched magnetized surface. Am J Appl Math. 2022;10(2):29. doi:10.11648/j.ajam.20221002.12.
25. Sakiadis BC. Boundary-layer behavior on continuous solid surface: i. boundary-layer equations for two-dimensional and axisymmetric flow. J AIChe. 1961;7:26–8. doi:10.1002/aic.690070108.

26. Tsou FK, Sparrow EM, Goldstain RJ. Flow and heat transfer in the boundary layer on a continuous moving surface. Int J Heat Mass Transf. 1967;10:219–35. doi:10.1016/0017-9310(67)90100-7.
27. Hussain S, Parveen R, Katbar N, Rehman S, Abd-Elmonem A, Abdalla N, et al. Entropy generation analysis of MHD convection flow of hybrid nanofluid in a wavy enclosure with heat generation and thermal radiation. Rev Adv Mater Sci. 2024;63(1):20240037. doi:10.1515/rams-2024-0037.
28. Lin Y, Rehman S, Akkurt N, Shedd T, Kamran M, Imran Qureshi M et al. Free convective trickling over a porous medium of fractional nanofluid with MHD and heat source/sink. Sci Rep. 2022;12:20778. doi:10.1038/s41598-022-25063-y.
29. Sharma R, Bisht A, Kumar A. Numerical study of fractional boundary layer flow over a stretching sheet with variable thickness: a finite difference approach. AIP Conf Proc. 2020;2253:020018. doi:10.1063/5.0018931.
30. Hosseini Z, Abidi A, Mohammadi S, Mehryan S, Hulme C. A fully resolved computational fluid dynamics study of the boundary layer flow of an aqueous nanoliquid comprising gyrotactic microorganisms over a stretching sheet: the validity of conventional similarity models. Mathematics. 2021;9(21):2655. doi:10.3390/math9212655.
31. Alam A, Marwat DNK, Ali A. Flow of nano-fluid over a sheet of variable thickness with non-uniform stretching (shrinking) and porous velocities. Adv Mech Eng. 2021;13. doi:10.1177/16878140211012913.
32. Rehman S, Rehman S, Khan A, Khan Z. The effect of flow distribution on heat and mass transfer of MHD thin liquid film flow over an unsteady stretching sheet in the presence of variational physical properties with mixed convection. Physica A. 2020;551:124120. doi:10.1016/j.physa.2019.124120.
33. Fatunmbi E, Okoya S, Makinde O. Convective heat transfer analysis of hydromagnetic micropolar fluid flow past an inclined nonlinear stretching sheet with variable thermo-physical properties. Diffus Found. 2020;26:63–77. doi:10.4028/www.scientific.net/DF.26.63.
34. Abbas N, Tumreen M, Shatanawi W, Qasim M, Shatnawi TA. Thermodynamic properties of second grade nanofluid flow with radiation and chemical reaction over slendering stretching sheet. Alex Eng J. 2023;70:219–30. doi:10.1016/j.aej.2023.02.031.
35. Cortell R. A numerical tackling on Sakiadis flow with thermal radiation. Chin Phys Lett. 2008;25(4):1340. doi:10.1088/0256-307X/25/4/048.
36. Kebede T, Haile E, Awgichew G, Walelign T. Heat and mass transfer analysis in unsteady flow of tangent hyperbolic nanofluid over a moving wedge with buoyancy and dissipation effects. Heliyon. 2020;6:e03776. doi:10.1016/j.heliyon.2020.e03776.
37. Pop I, Ingham DB. Convective heat transfer: mathematical and computational modelling of viscous fluids and porous media. 1st ed. New York: Pergamon; 2001.